

Proceedings

Shotcrete for Underground Support XI

Engineering Conferences International

Year 2009

NON-LINEAR, ELASTIC - PLASTIC
RESPONSE OF STEEL FIBRE
REINFORCED SHOTCRETE TO
UNIAXIAL AND TRIAXIAL
COMPRESSION TESTING

Hla Aye Saw*
Christopher R. Windsor‡

Ernesto Villaescusa†
Alan G. Thompson**

*Western Australian School of Mines, Curtin University of Technology,
h.saw@curtin.edu.au

†Western Australian School of Mines, Curtin University of Technology,
E.Villaescusa@curtin.edu.au

‡Western Australian School of Mines, Curtin University of Technology,
Chris.Windsor@curtin.edu.au

**Western Australian School of Mines, Curtin University of Technology,
A.Thompson@curtin.edu.au

This paper is posted at ECI Digital Archives.

<http://dc.engconfintl.org/shotcrete/8>

NON-LINEAR, ELASTIC - PLASTIC RESPONSE OF STEEL FIBRE REINFORCED SHOTCRETE TO UNIAXIAL AND TRIAXIAL COMPRESSION TESTING

Hla Aye Saw, CRC Mining, WA School of Mines, Curtin University of Technology,
Locked Bag 30, Kalgoorlie, Western Australia, WA6433, Australia
T:+61 08 90886099, F:+61 08 90886151, h.saw@curtin.edu.au

Ernesto Villaescusa, CRC Mining, WA School of Mines,
Curtin University of Technology,

Christopher R. Windsor, CRC Mining, WA School of Mines,
Curtin University of Technology,

Alan G. Thompson, CRC Mining, WA School of Mines,
Curtin University of Technology,

ABSTRACT

Understanding the complete stress-strain behavior of shotcrete is extremely important in ground support design; especially in cases where large deformations are expected such as around mine excavations at great depth. The application of non-linear numerical modeling to mining industry problems has increased in recent years. More realistic stress-strain response and failure criteria in complex plasticity models are also being used in the design of the larger, deeper mines. One of the factors to improve the reliability of numerical modeling is to properly define geotechnical parameters for both the rock mass and shotcrete surface support. Uniaxial and triaxial compression tests on steel fibre reinforced shotcrete (SFRC) have been used to quantify elastic-plastic response behaviour for both the peak and post-peak regions. The laboratory tests were conducted with a servo-controlled testing machine to obtain complete stress-strain curves. The test results include unconfined and triaxial compressive strength, shear strength and tensile strength together with the elastic and plastic mechanical properties of SFRC. A method is also suggested for obtaining the plasticity parameters for non-linear modeling of SFRC.

1. INTRODUCTION

The theory of plasticity is the name given to the mathematical study of stress and strain in plastically deformed solids (Hill, 1950). Hill published the book "Mathematical theory of plasticity" based mainly on the test results of metals. However, he did suggest that the theory may apply to other potentially plastic materials. Since that time, extensive research and development has been conducted on the application of plasticity theory to other materials such as soils, rocks, concrete and shotcrete. To date, the theory has reached a good degree of maturity for application to geomaterials, although further progress is still expected (Yu, 2006). At the same time the continual development of testing equipment,

computing methods, software and hardware enhance the application of plasticity theory.

Shotcrete is a designed material with anisotropic, inhomogeneous and elastic-plastic behaviour. Therefore, understanding of the complete stress-strain behavior of shotcrete is extremely important in ground support design; especially in cases where large deformations are expected such as around mine excavations at great depth. A rock mass is naturally Discontinuous, Anisotropic, Inhomogeneous and No-Elastic (DIANE), (Harrison & Hudson, 2000). When a rock mass deforming non-linearly, the shotcrete also responds non-linearly. Deformation mechanisms of shotcrete which support the rock mass surface excavated by drill and blast methods are described in Windsor (1999).

2. GEOTECHNICAL PARAMETERS

Many parameters are required for non-linear elastic-plastic numerical modeling for the rock mass and rock improvement system (rock bolts, shotcrete and wire mesh). The fundamental material parameters include; Young's modulus, Poisons ratio, uniaxial compressive strength, shear strength (both peak and residual c and ϕ), tensile strength, dilation angle (ψ) and strain rate at peak and residual stress. In addition, account need to be taken of the geological conditions to cooperate major and minor structures, stresses and hydrology. The only parameters vary according to the models implicated with the software. Only the parameters directly derived from the laboratory test results are presented. The laboratory test results are presented as simple stress-strain curves. No numerical modeling was attempted to correlate with the test results. The stress-strain curves are presented as raw data.

3. A COMPLETE STRESS-STRAIN RELATION

In the elastic region the strains are linearly related to the stress as assumed in Hooke's Law (Hooke, 1705). In the elastic region strains are uniquely determined by stresses and can be computed directly using Hooke's law without any regard to how the stress state was attained. Mathematically, elastic strain and stress can be simply written as:

$$\varepsilon^e = \frac{\sigma}{E} \quad (1)$$

Where, ε^e is elastic strain, σ is stress and E is Young's modulus.

In the plastic region, the strains are not uniquely determined by the stresses but depend on the whole history of loading or how the stress state was reached. An essential part of plasticity theory is to define when the material starts to deform or yield. A failure criterion is used to describe by point at which fracture or yield occurs. The criterion under which yield occurs is called a yield criterion. The most widely used yield criterion is the Coulomb yield criterion (Coulomb, 1776),

$$\tau = c + \sigma_n \tan \phi \quad (2)$$

Where, τ and σ_n represent shear stress and normal stress, respectively. The parameters c and ϕ are assumed to be constants called the cohesion and the angle of internal friction. In reality c and ϕ change with stress level. Once the yield criterion is satisfied, the material will flow obeying the flow rule. The flow rule is termed associated if the plastic strains are associated directly with the yield surface and if not it is termed non-associated. The non-associated flow rule states that the plastic strain rate is proportional to the derivatives of the plastic potential with respect to the corresponding stress. This can be described by the following equation.

$$\dot{\epsilon}^p = \lambda \frac{\partial g}{\partial \sigma} \quad (3)$$

Where, $\dot{\epsilon}^p$ is plastic strain increment, λ is Lagrange or plastic multiplier and g is a plastic potential. The definition of plastic potential function “ g ” suggested by Radenkovic [1961] is,

$$g = \tau - \sigma \sin \psi + \text{constant} \quad (4)$$

where, ψ is the dilation angle. A dilation angle is defined as the ratio of plastic volume change over plastic shear strain (Hansen, 1958). The direction of deformation which lies at a dilation angle above the shearing surface is shown in Figure 1.

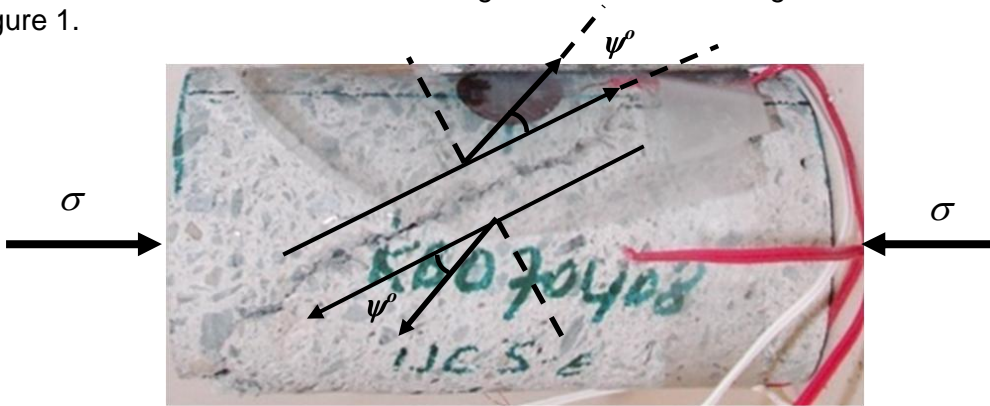


Figure 1. Shearing and dilation.

For the Mohr-Coulomb yield criterion, equation (4) can be written in terms of principal stresses for triaxial test conditions where, $\sigma_2 = \sigma_3$,

$$g = \frac{1}{2}(\sigma_3 - \sigma_1) + \frac{1}{2}(\sigma_3 + \sigma_1) \sin \psi + \text{constant} \quad (5)$$

The principal plastic strain rates are obtained by differentiating equation (5) with respect to the principal stresses as given in equation (3).

$$\begin{bmatrix} \dot{\varepsilon}_1^p \\ \dot{\varepsilon}_2^p \\ \dot{\varepsilon}_3^p \end{bmatrix} = \lambda \begin{bmatrix} \frac{1}{2}(1 + \sin\psi) \\ \frac{1}{2}(-1 + \sin\psi) \\ \frac{1}{2}(-1 + \sin\psi) \end{bmatrix} \quad (6)$$

From which,

$$\dot{\varepsilon}_v^p = \lambda \sin\psi \quad (7)$$

$$\dot{\varepsilon}_1^p = \lambda \frac{1}{2}(1 + \sin\psi) \quad (8)$$

By eliminating λ from equations (7) and (8), $\sin\psi$ is given by,

$$\sin\psi = \frac{\dot{\varepsilon}_v^p}{2\dot{\varepsilon}_1^p + \dot{\varepsilon}_v^p} \quad (9)$$

This equation for $\sin\psi$ can be expressed as,

$$\sin\psi = \frac{\dot{\varepsilon}_v^p / \dot{\varepsilon}_1^p}{2\dot{\varepsilon}_1^p / \dot{\varepsilon}_v^p + \dot{\varepsilon}_v^p / \dot{\varepsilon}_v^p} \quad (10)$$

or

$$\sin\psi = \frac{1}{\frac{2\dot{\varepsilon}_1^p}{\dot{\varepsilon}_v^p} + 1} \quad (11)$$

$\dot{\varepsilon}_v^p / \dot{\varepsilon}_1^p$ give the slope of volumetric – axial strain curve. Therefore, the inverse of the slope can be substituted into equation (11) to obtain the dilation angle ψ .

The total strain, ε^t the sum of elastic and plastic strains, may written as,

$$\varepsilon^t = \varepsilon^e + \varepsilon^p \quad (12)$$

Typical complete stress-strain curves obtained from uniaxial and triaxial compression tests on steel fibre reinforced shotcrete are shown in Figure 2. The broken lines show the result obtained using strain gages on the specimens and the solid lines shows the calculated strain from the displacement measurements between the top and bottom of the test machine platens.

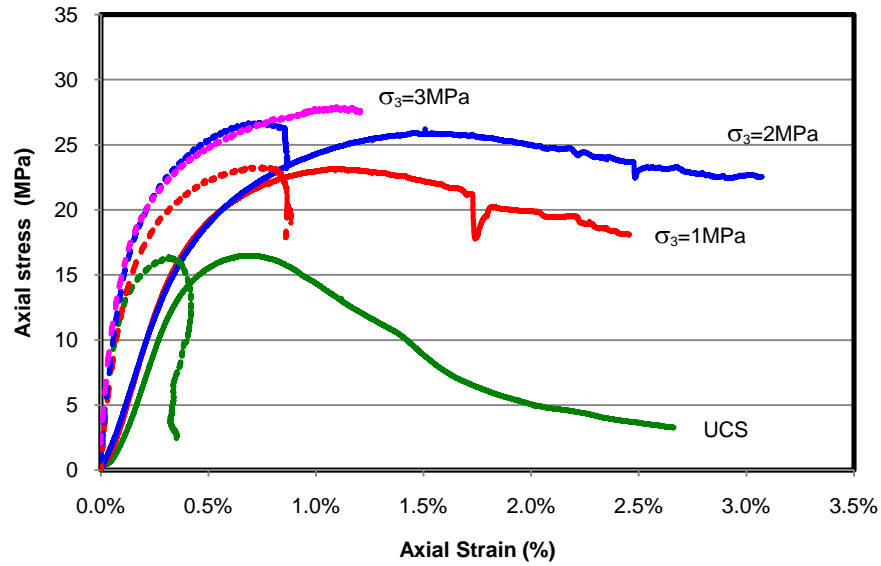


Figure 2. A typical stress-strain response of SFRS at different confining pressure.

4. MIX DESIGN AND CURING METHOD

The wet mix shotcrete used in these investigations is similar to that used at the one of underground gold mines in Eastern Gold Fields region, Kalgoorlie, Western Australia. Shotcrete panels were sprayed on site and delivered to the WASM geomechanics laboratory on the same day. The specimen were cored from the panels and stored in a curing chamber, which was set at 30°C and 90% humidity. The tests were conducted on three batches of samples after at four different curing periods (1, 3, 7 and 28 days). All of the shotcrete batches have the same mix design which given in Table 1.

Table 1. Mix design of SFRS used in this research.

Material	Quantity for 1 m ³ mix
Cement (GP)	400 kg
Coarse aggregate (7-10 mm)	220 kg
Crusher dust	1300 kg
Sand	1640 kg
Water	150 L
Steel fibres	30 kg
Liquid Meyco (MS 685)	11 L
Delvo Stabiliser	5 L
Rheobuild 1000	8 L
Pozzolith 322Ni	1.3 L
Accelerator	4% of cement

5. RESULTS AND DISCUSSION

5.1 Uniaxial compressive test

These tests were performed using an Instron, servo controlled hydraulic testing machine. The loading rate of the machine was set at 0.12 mm/min. The strains were measured with two biaxial foil strain gages with 10 mm gage length that were installed diametrically at specimen mid-height. Figure 3 shows a shotcrete sample before and after testing. The test results are summarised in Table 2. The stress-strain curves are shown in Figure 4.



Figure 3. Shotcrete sample before and after UCS test.

Table 2. Summary of UCS test with complete stress-strain measurement.

Batch No.	Curing (Days)	UCS σ_c (MPa)	Elastic properties					
			Young's modulus			Poisson's ratio		
			E_{t50} (GPa)	E_s (GPa)	E_a (GPa)	ν_{t50}	ν_s	ν_a
1	1	16.2	-	-	-	-	-	-
2	1	18.1	14	15	14	0.36	0.31	0.42
3	1	18.3	11	16	11	0.20	0.28	0.19
1	3	23.4	-	-	-	-	-	-
2	3	18.3	12	15	12	0.28	0.29	0.28
3	3	22.9	9	13	8	0.16	0.21	0.16
1	7	28.5	-	-	-	-	-	-
2	7	23.2	16	21	16	0.23	0.34	0.22
3	7	25.7	14	17	14	0.17	0.29	0.17
1	28	32.8	15	21	14	0.21	0.31	0.21
2	28	27.2	18	28	17	0.30	0.29	0.29
3	28	31.5	11	16	10	0.17	0.22	0.15

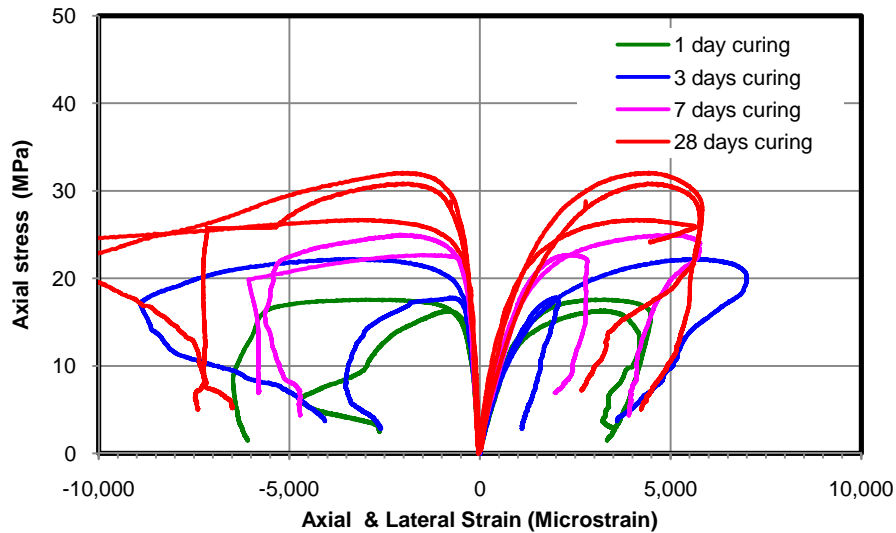


Figure 4. Stress versus strain curves from UCS test.

The test results show that UCS increases with curing time and that Young's modulus and Poisson's ratio do not change significantly. The yield point of the curves increased with increasing UCS. After yield, non-linear strain hardening can be observed until it reaches peak. After peak, localized damage develops and strain softening and/or the "snap-back" begins. The "snap-back" implies that the materials failed in brittle mode. Globally, the SFRS continued to deform in shear associated with dilation with the load taken by steel fibres. The effective steel fibres are those which span the failure surface and are firmly anchored on both sides. The post-peak behaviour of SFRS is highly dependent on the numbers and orientation of the effective fibres. Figure 5 shows that effective steel fibres with various orientations respond in different modes. The responses are predominantly shear, tensile and compression in nature. The most common response is a combination of these modes. The force-displacement relationship of the individual fibres can be described with characteristic diagrams as shown in Figure 6.

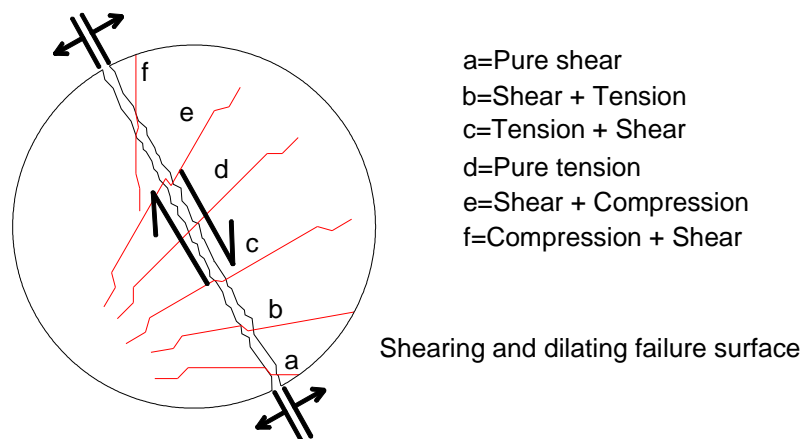


Figure 5. Effective fibre with various response modes for different fibre orientation. (Modified from Windsor, 1996)

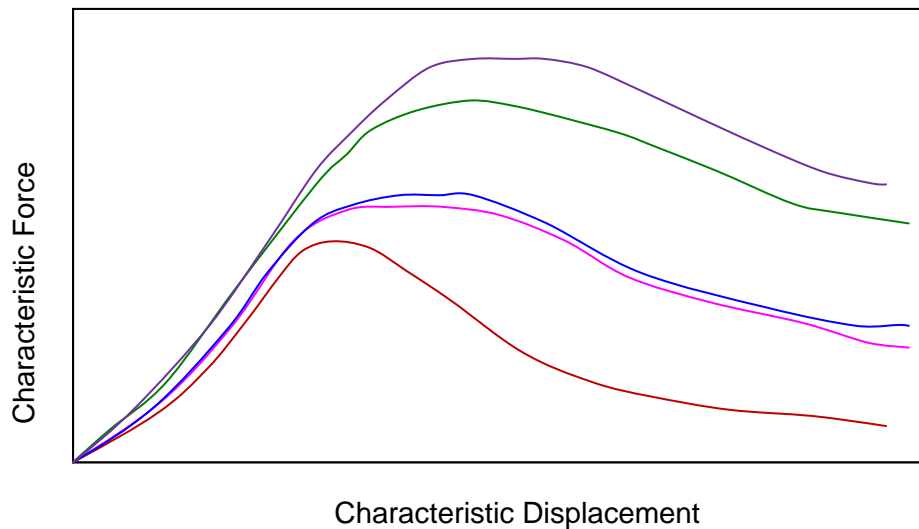


Figure 6. Force-displacement characteristic diagram for different fibre orientation.

5.2 Indirect tensile strength test (Brazilian method)

The tensile strength was obtained according to the test method suggested by International Society of Rock Mechanics (ISRM) (Fairhurst & Hudson, 1999). The test was performed with Avery universal testing machine. Load and displacement were monitored and stored at resolutions of 0.01kN and 0.02mm, respectively. Figure 7 shows a sample after a Brazilian test. Similar to the UCS tests, the tensile strength also increases with curing age. The summary of Brazilian test results is given in Table 3. Figure 8 shows the load-displacement curves for indirect tensile strength tests. The results suggested that, after first crack the load is taken by the effective fibres and the ultimate tensile strength depends on the numbers and orientation of the effective fibres. Figure 9 shows the correlation between the UCS and the peak tensile strength. The correlation suggests that the peak tensile strength of SFRS is about 15% of UCS.



Figure 7. Samples after Brazilian test.

Table 3. Summary of Brazilian test results.

Batch No.	Curing (days)	Peak tensile strength (MPa)
3	1	2.4
3	1	2.5
2	3	3.4
3	3	2.8
3	3	4.3
3	3	3.5
2	7	4.4
2	7	4.0
3	7	3.6
3	7	2.8
3	7	3.2
1	28	5.5
1	28	4.0
2	28	4.9
3	28	5.4
3	28	5.1
3	28	4.8

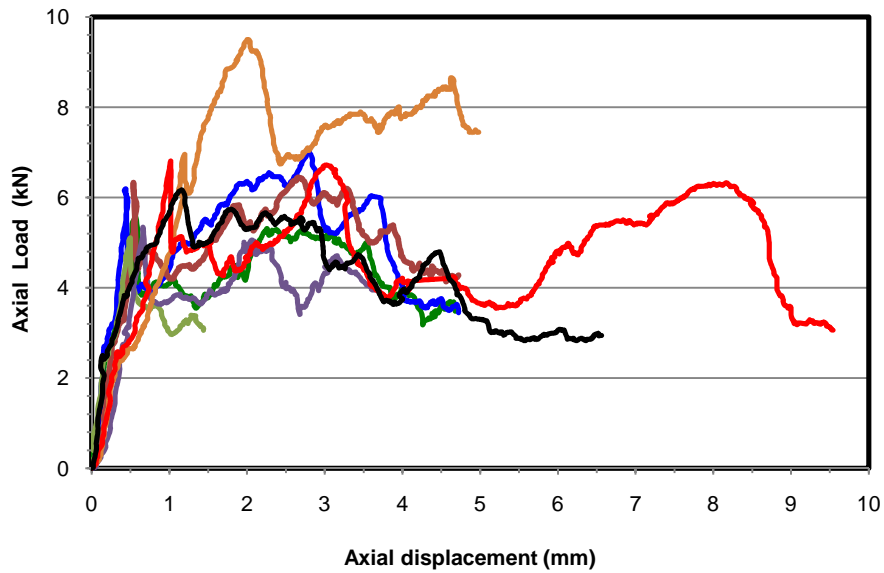


Figure 8. Load-displacement curves from Brazilain tests.

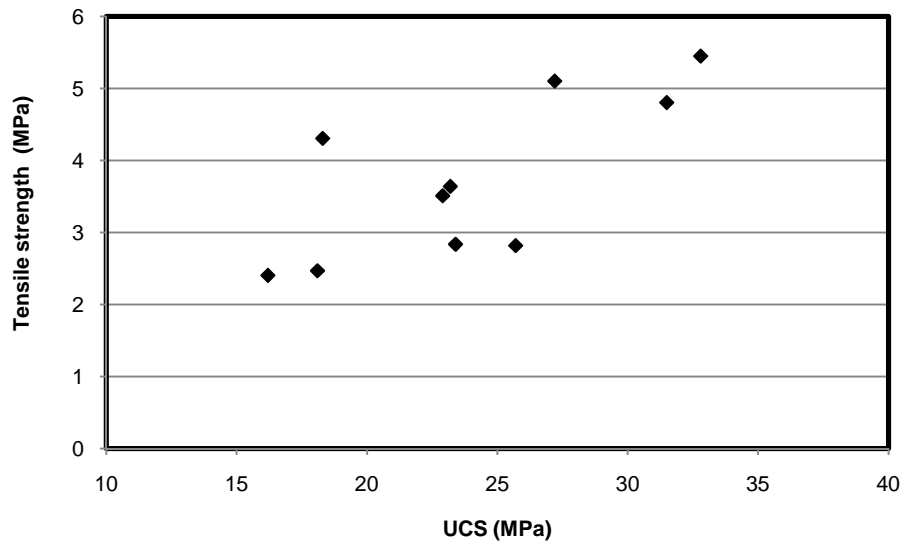


Figure 9. Correlation of peak tensile strength and UCS.

5.3 Shear strength and dilation angle

The triaxial compression test is a useful test method to obtain complete stress-strain response of the SFRS sample and to derive the strength parameters and dilation angles. In these investigations, tests were performed using the Instron testing machine. Three different confining pressures 1, 2 and 3 MPa were applied to three specimens. The strains were also measured with two biaxial foil strain gages with 10 mm gage length, which were also installed diametrically at specimen mid-height. Figure 10 shows SFRS samples after triaxial compression testing. A summary of test results is given in Table 4. The peak and residual strength envelopes plotted on the p-q plane are shown in Figure 11 and 12 respectively. Generally, the shear strength increased with curing time. The friction and dilation angle do not change significantly with curing time. The residual strength is influenced by confining pressure. Main course of increase in strength was in increase in cohesion, the slope of the lines associated with friction angle were very similar.

The stress-strain curves shown in Figure 13 to 15 can be used to calculate the plastic strain rate at peak and residual using the total strain equation (12). The plastic strain increased with increased confining pressure. The peak stress does not change significantly from 1 day to 7 days curing but significantly increased at 28 days. The dilation angles are calculated from the axial and volumetric strain curves and are given in Figures 16 to 18. The correlation of friction and dilation angle is shown in Figure 19. This suggests that, higher dilation occurred in samples with lower friction angle. Also, the amount of dilation decreases with increasing confining pressure.



Figure 10. Samples after triaxial test.

Table 4. Summary of Triaxial test results.

Batch No.	Curing (Days)	Shear strength				Average dilation angle, ψ°
		Peak		Residual		
		C (MPa)	ϕ°	C (MPa)	ϕ°	
1	1	4	38	-	-	-
2	1	4	45	2	45	8
3	1	5	36	5	32	13
1	3	5	40	3	42	-
2	3	4	40	3	41	10
3	3	6	38	-	-	12
1	7	8	35	5	35	-
2	7	5	40	4	41	10
3	7	6	40	5	38	10
1	28	8	38	7	18	12
2	28	11	18	-	-	12
3	28	8	38	-	-	10

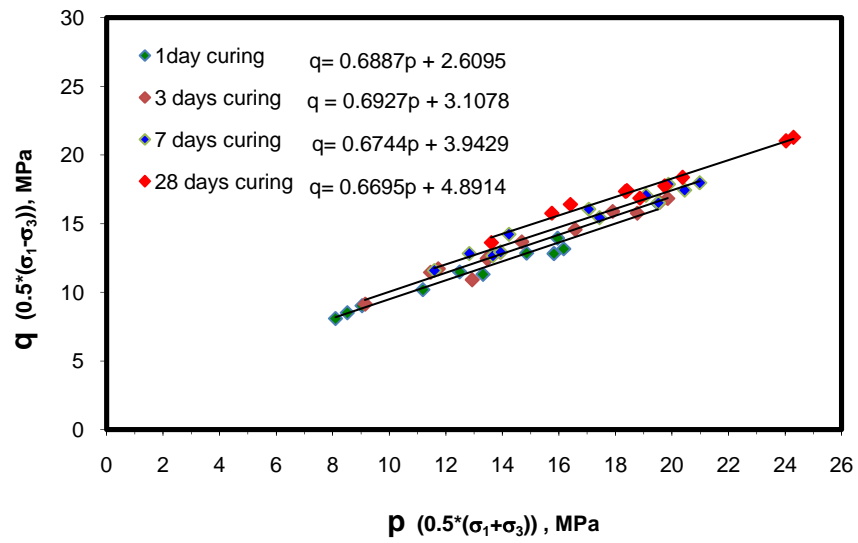


Figure 11. Peak shear strength envelopes plotted on the p-q plane.

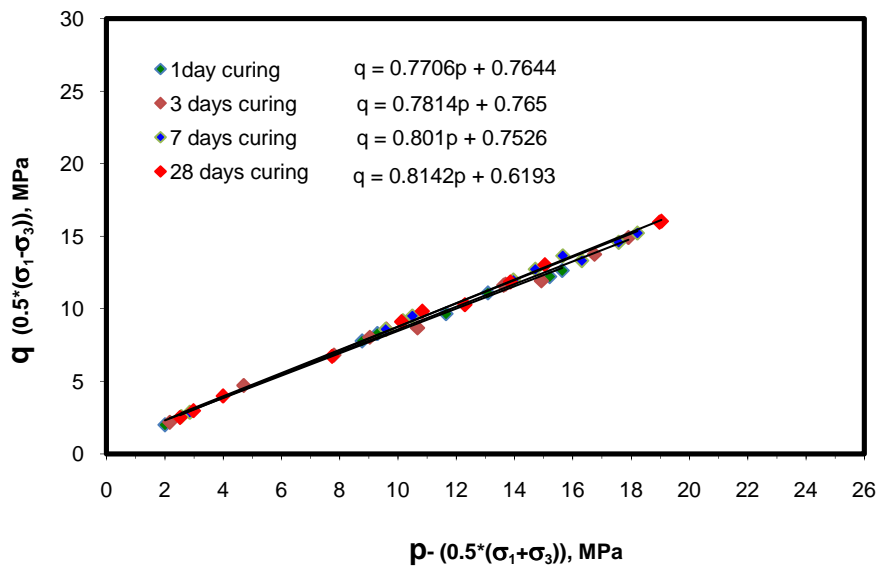


Figure 12. Residual shear strength envelopes plotted on the p-q plane.

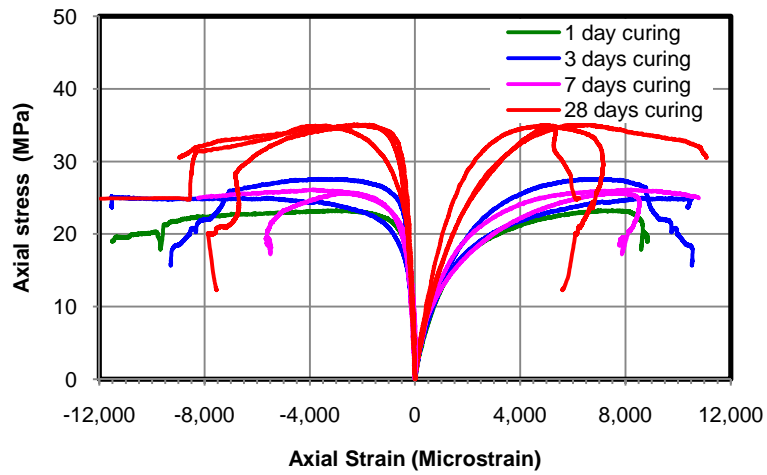


Figure 13. Axial stress versus strain curves at 1 MPa confinement.

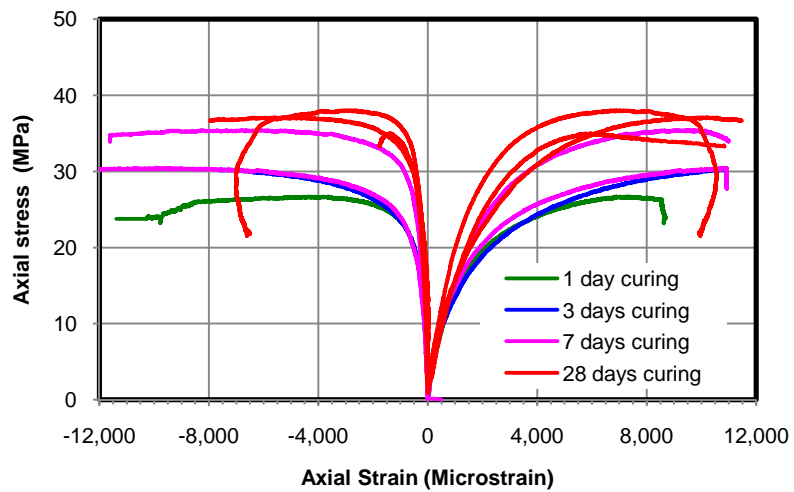


Figure 14. Axial stress versus strain curves at 2 MPa confinement.

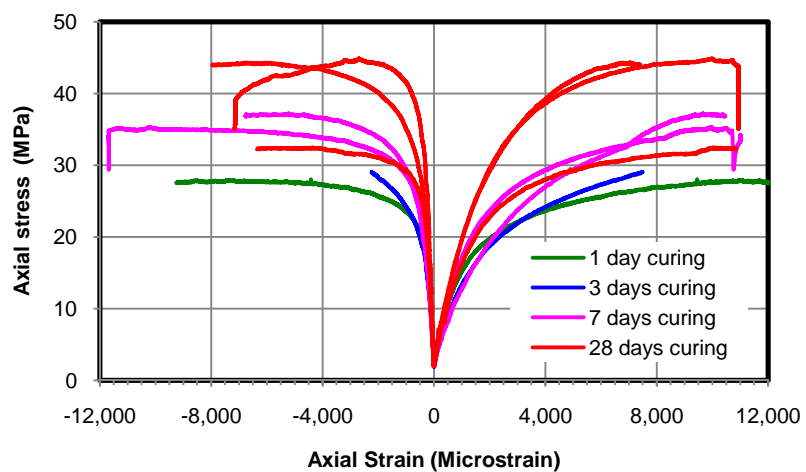


Figure 15. Axial stress versus strain curves at 3 MPa confinement.

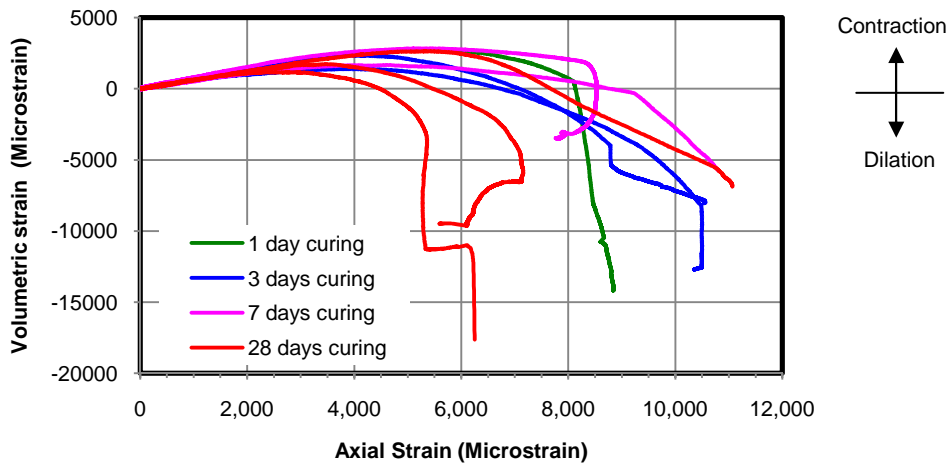


Figure 16. Volumetric versus axial strain curves at 1 MPa confinement.

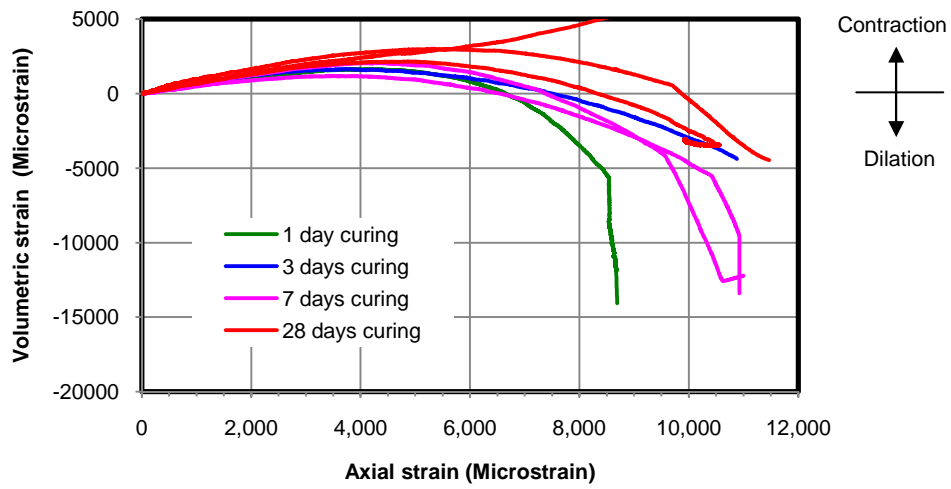


Figure 17. Volumetric versus axial strain curves at 2 MPa confinement.

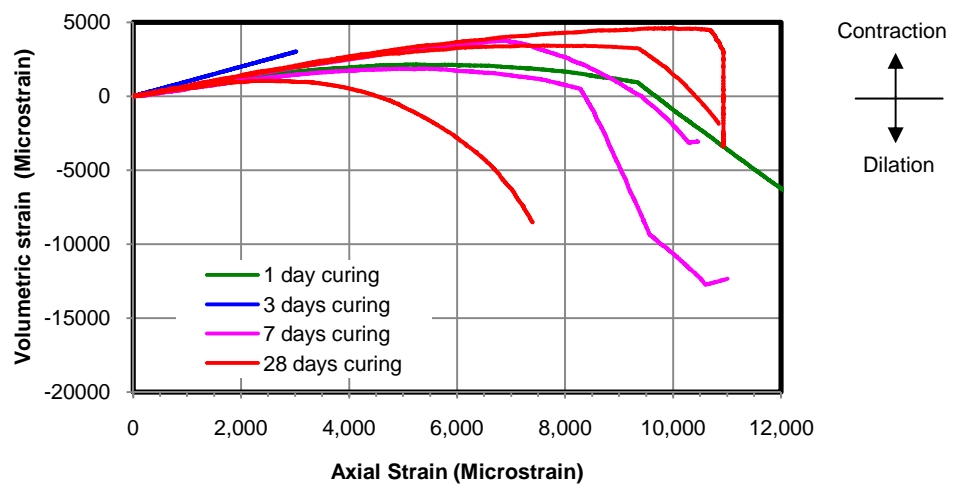


Figure 18. Volumetric versus axial strain curves from at 3 MPa confinement.

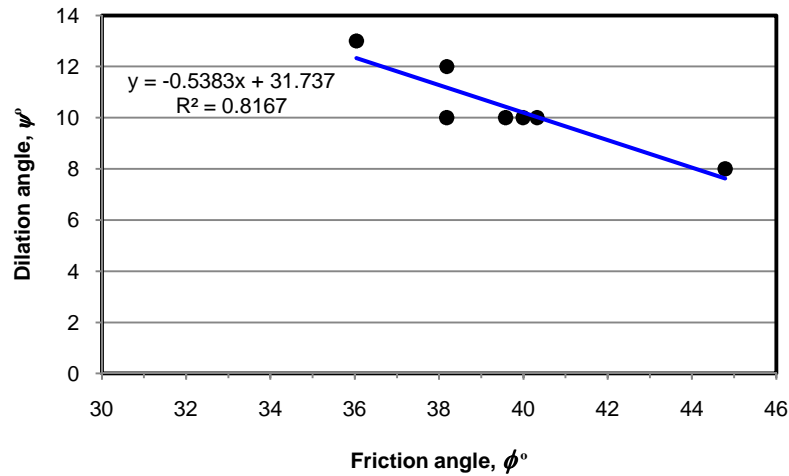


Figure 19. Correlation between the friction angle and the dilation angle.

6. SUMMARY AND INTERPRETATION OF RESULTS

Based on the results, the following conclusions can be drawn for the mix tested:

- The average UCS at 1, 3, 7 and 28 days curing were 18, 22, 26 and 31 MPa respectively.
- The average tensile strength at 1, 3, 7 and 28 days curing were 2, 4, 4 and 5 MPa respectively.
- The tensile strength is about 15% of UCS.
- The average Young's modulus at 1, 3, 7 and 28 days curing were 13, 10, 15 and 14 GPa respectively.
- The average Poisson's ratio at 1, 3, 7 and 28 days curing were 0.3, 0.2, 0.2 and 0.2 respectively.
- The average peak cohesion at 1, 3, 7 and 28 days curing were 4, 5, 6 and 9 MPa respectively.
- The average peak friction angle at 1, 3, 7 and 28 days curing were 40, 39, 38 and 31 degree respectively.
- The average residual cohesion at 1, 3, 7 and 28 days curing were 4, 3, 5 and 7 MPa respectively.
- The average residual friction angle at 1, 3, 7 and 28 days curing were 39, 42, 38 and 18 degree respectively.

- The residual strength is influenced by the confining pressure as the specimen responded in continuously strain hardening after post peak.
- The dilation angle ranges from 8 to 13 degrees and does not change significantly with curing time. It decreases with increasing friction angle. The amount of dilation decrease with increasing confining pressure.
- A complete stress-strain response can be subdivided into linear elastic and non-linear plastic regions. The non-linear plastic region includes strain hardening up to the post peak (which plateau at high confining pressure), snap-back or/and strain softening after post peak.
- A snap-back occurs when the SFRS responds locally in the brittle mode.
- The post peak behavior is influenced by the confining pressure and the number and orientation of effective fibres.

A test programme was conducted on steel fibre reinforced shotcrete (SFRC) samples to define the mechanical parameters for non-linear, elastic-plastic modelling. In particular, uniaxial and triaxial compression tests and Brazilian tests have been used to quantify elastic-plastic response behaviour for both the pre-peak and post-peak regions.

ACKNOWLEDGEMENTS

The writers wish to thank to Barrick Gold of Australia Limited for their funding and for supplying the steel fibre reinforced shotcrete sample slabs.

NOTATION

σ_1	= Major principal stress (Axial stress in triaxial test)
σ_2	= Intermediate principal stress (Confining pressure in triaxial test)
σ_3	= Minor principal stress (Confining pressure in triaxial test)
ε^t	= Total strain
ε^e	= Elastic strain
ε^p	= Plastic strain
ε_1^p	= Major plastic strain increment
ε_2^p	= Intermediate plastic strain increment
ε_3^p	= Minor plastic strain increment
ε_v^p	= Volumetric strain increment
τ	= Shear stress
σ_n	= Normal stress
c	= Cohesion
ϕ	= Friction angle

λ	= Plastic multiplier
g	= Plastic potential
ψ	= Dilation angle
E_{t50}	= Tangent Young's modulus
E_s	= Secant Young's modulus
E_a	= Average Young's modulus
ν_{t50}	= Tangent Poisson's ratio
ν_s	= Secant Poisson's ratio
ν_a	= Average Poisson's ratio

REFERENCES

- Brady, B.H.G., & Brown, E.T. (1993). *Rock mechanics for underground mining, Second edition*. London: Chapman & Hall.
- Coulomb, C. A., (1776). *Essais sur une application des regles des maximis et minimis à quelques problems de statique relatifs à l'architecture*. Mem. Acad. Roy. Pres. Divers, Sav. 5, 7, .
- Davis, R. O., & Selvadurai, A. P. (2002). *Plasticity and Geomechanics*. Cambridge: Cambridge University Press.
- Fairhurst, C. E., & Hudson, J. A. (1999). Draft ISRM suggested method for the complete stress-strain curve for intact rock in uniaxial compression. *International Journal of Rock Mechanics and Mining Science* , 279-289.
- Hansen, C. E.B., (1958). Line ruptures regarded as narrow rupture zones - Basic equations based on kinematic considerations. *Brussels conference 58 on Earth Pressure Problem*.
- Harrison, J. P., & Hudson, J. A. (2000). *Engineering Rock Mechanics:Part 2*. Oxford: Elsevier.
- Heyman, J. (1972). *Coulomb's Memoir on Statics: An Essay in the History of Civil Engineering*. Cambridge: Cambridge University Press.
- Hill, R. (1950). *The Mathematical Theory of Plasticity*. London: Oxford University Press.
- Hooke, R. (1705). *The posthumous Works, Containing his Cutlerian Lectures, and other Discourses, Read at the Meeting of the Illustrious Royal Society*. London: Samuel Smith and Benjamin Walford for Richard Waller.
- Radenkovic, D. (1961). Théorèmes limites pour un matériau de Coulomb à dilation non standardisée. *C.R. Ac.Sc.* 252, (pp. 4103-4104). Paris.
- Vermeer, P.A., & de Borst, R. (1984). Non-associated plasticity for soils, concrete and rock. *Heron Vol.29. No.3* , 3-64.
- Windsor, C. R. (1996). Rock reinforcement systems. *Int. J. Rock. Mech. Min. Sc. & Geomech.* V34, 6 , 919-951.
- Windsor, C. R. (1999). Structural design of shotcrete linings. *Australian Shotcrete Conference and Exhibition* (p. 32). Sydney: IBC Conference.
- Yu, H.-S. (2006). *Plasticity and Geotechnics*. New York: Springer Science and Business Media.